Development of an AMB Energy Storage Flywheel for Industrial Applications

Larry Hawkins[1] and Eric Blumber

Calnetix, Inc.

12880 Moore Street, Cerritos, CA 90703, USA

Andy Paylan

Vycon, Inc.

7th International Symposium on Magnetic Suspension Technology

Abstract. *The development and testing of an AMB supported, 125 kW energy storage flywheel is discussed. The flywheel is being developed for a number of industrial applications to provide: 1) ride-through power, 2) voltage support in rail applications, 3) power quality improvement, and 4) UPS service in-lieu of standby batteries. The flywheel, which operates in a vacuum, is supported by AMBs to minimize bearing losses, and has a high power motor/generator coupled to an efficient power conversion module. The magnetic bearing system is designed to minimize losses for both energy storage efficiency and to reduce heat generated on the rotating assembly. The magnetic bearing controller uses gain scheduling to stabilize the gyroscopic rotor and uses synchronous cancellation to minimize dynamic loads. Dynamic data from high speed testing is presented. Rotor temperature measurements from thermal equilibrium testing are presented and discussed.*

Keywords: energy storage flywheel, magnetic bearings, UPS

1. Introduction

A flywheel energy storage system is being developed for industrial applications. The flywheel based storage system is targeted for some applications where the characteristics of flywheels offer advantages over chemical batteries: 1) ride-through power in turbine or diesel generator sets, 2) voltage support in rail applications, 3) power quality improvement, and 4) uninterruptible power supplies (UPS). Some of the key advantages offered by flywheels compared to batteries are: 1) life is unaffected by frequent deep discharge and charge cycles, or by high discharge and charge rates, 2) no routine maintenance is required, 3) they are relatively insensitive to high ambient temperatures, 4) less floor space is required and energy density is higher for flywheels, and 5) they have none of the environmental concerns with eventual disposal that arise with lead-acid batteries.

Flywheel based systems are particularly advantageous in UPS systems when combined with diesel or turbine generator sets (gensets). In order to protect against prolonged outages, all mission critical applications require the installation of gensets to ensure continuous operation once the typical 10-minute battery life is exhausted. With 90% of all power quality events lasting less than 3 seconds and the ones lasting more than 3 seconds almost always causing outages lasting in hours rather than minutes, flywheel based UPS systems make sense for the entire spectrum of power quality events. Energy stored in the flywheel is used for events lasting less than 15 seconds. For longer events, the flywheel supplies ride-through power while the genset is being brought on line to provide long-term power.

The ability of flywheel systems to quickly charge and discharge is a key enabling technology for applications requiring pulse power. One such application is the charging of

[1]Contact author: larry@calnetix.com

the flywheel through the energy dissipated in the deceleration of a railway car and discharging the captured energy in the acceleration of the car. Traditional chemical batteries cannot be used in this application due to the lapse in first charging the batteries (chemical reaction delays) and then discharging the batteries, once again chemical reaction delays. Additionally, this type of service severely reduces battery life, but has no effect on flywheel life.

The flywheel system under development consists of two major subsystems: 1) the flywheel module, which includes the flywheel, motor/generator, and a five axis active magnetic bearing system, and 2) a three-phase bi-directional IGBT bridge (converter) used for both motoring and generation. The output and input to the flywheel system is through a DC bus into and out of the converter. The converter creates a sine wave drive from the DC bus to drive the flywheel during motoring, and converts the varying sinusoidal frequency from the flywheel to DC during generation. Details of the converter were reported in [1]. The design of the flywheel module is reported here.

The flywheel module, shown in Figure 1, is designed to store 1.25 kWh at 36,000 rpm and deliver 125kW (160 kVA) for more than 15 seconds. In many flywheel designs that have been suggested, the goal of maximizing energy density has lead to carbon fiber composites as the material choice for the flywheel hub. This can result in an expensive design, and some difficult design tradeoffs. A key design goal for this industrial flywheel was to keep the cost for the flywheel system at or below the cost of an battery system with the same peak power. This goal leads to high strength steel as the material of choice for the flywheel hub. To maximize efficiency, the flywheel rotor operates in a vacuum and uses magnetic bearings. Thus rotor heat removal must be accomplished through radiation, making minimization of rotor heating a major design consideration. Consequently, low-loss homopolar, permanent magnet bias magnetic bearings and a permanent magnet motor/generator were chosen to reduce rotor heating. Thermal testing is now underway and initial results are reported here.

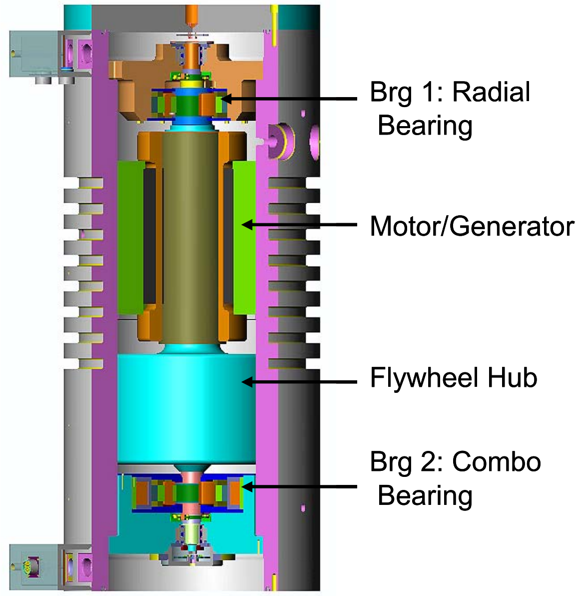

Fig. 1. Flywheel Cross-Section

2. Energy Storage Flywheel

The vertically mounted flywheel (Figure 1) uses a steel flywheel placed below a separate motor/generator on the same shaft. This partially integrated configuration was chosen to allow integration of an existing, proven motor/generator with a robust flywheel design. Similar configurations have been well tested and proven to be reliable [2]-[4]. Although the flywheel hub has a fairly high Ip/It, the rigid body Ip/It for the entire flywheel rotor is quite low (0.25) due to the size of the high-power density motor/generator. This feature helps to simplify the magnetic bearing control. The motor/generator utilizes a two-pole permanent magnet rotor designed by Calnetix. The magnet is captured radially by a thick non-magnetic sleeve, which also provides the structural connection to the rest of the flywheel rotor. The magnetic bearings are placed immediately above the motor/generator and immediately below the flywheel. Rolling element backup bearings are placed outboard of the magnetic bearings.

2.1 Motor/Generator

The flywheel motor/generator incorporates a radially polarized permanent magnet (PM). PM machines uses permanent magnets to provide field excitation, providing high efficiency and reduced size for an equivalent power when compared with other types of machines such as induction and switched reluctance machines. The motor/generator consists of a rotor assembly and a stator assembly. The rotor assembly contains the permanent magnets, which are constrained by an inconel retaining sleeve. The sleeve also provides the structural connection between the flywheel and the upper bearing shaft. The three-phase stator is conventionally wound, allowing a simple low cost construction. To ensure effective operation in the vacuum environment, the motor/generator design was optimized to minimize rotor losses due to tooth ripple effects and armature current harmonics.

2.2 Magnetic Bearing

The magnetic bearings use a homopolar, permanent magnet bias topology. Homopolar refers to the direction of the bias flux, which is oriented either uniformly into or uniformly out of the shaft at any circumferential location. This topology significantly reduces rotor eddy current losses compared to conventional designs. A permanent magnet is used to produce the bias flux for the bearing, resulting in several advantages compared to electromagnetic bias: 1) less power is consumed by the magnetic bearings and 2) the bearing has a more linear force/displacement characteristic due to the contribution of the large, fixed reluctance of the permanent magnet to the bias flux path.

The radial bearing (Brg 1 in Figure 1) is a two-axis radial bearing. The combo bearing (Brg 2) is a three-axis combination radial/thrust bearing. The basic operation of this bearing topology was described in [5]. A combination bearing is more compact axially than separate radial and axial magnetic bearings. This increases the frequency of the rotor bending modes, making the magnetic bearing control design less difficult. This combination bearing, shown in more detail in Figure 2, uses a single radially polarized permanent magnet ring to provide bias flux for both the radial and axial flux paths. Three separate pairs of control coils allow individual control of each axis (two radial and one axial).

Some characteristics of the magnetic bearings are given in Table 1.

Table 1. Magnetic Bearing Characteristics

Bearing	*Radial Bearing*	*Combo Radial*
Bearing Ref Name	Brg 1	Brg 2
Coordinate Names	x1,y1	x2,y2
Load Capacity, N (lbf)	555 (125)	555 (125)
Force Constant, N/A (lbf/A)	77 (17.3)	77 (17.3)
Negative Stiffness, mm (lbf/in)	1050 (6,000)	1050 (6,000)
Air Gap, mm (in)	0.508 (.020)	0.508 (.020)
Maximum Current, A	7.2	7.2

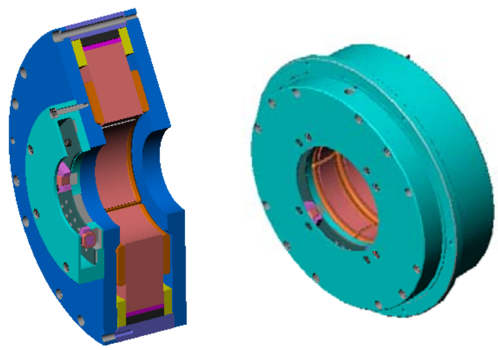

Fig. 2. Combination Magnetic Bearing

2.3 Backup Bearings

The backup bearings have radial and axial clearances of 0.20 mm (less than one-half of the magnetic air gap) between the bearing inner races and the shaft. The backup bearings are expected to carry load in the following cases: 1) when the system is at rest and the magnetic bearings are turned off, 2) in the event of a substantial shock transient that exceeds the capacity of the magnetic bearings, and 3) in the event of a component failure that causes the loss of one more axes of control for the magnetic bearing.

The backup bearing system consists of a duplex pair of angular contact ball bearings at each end of the shaft. The lower backup bearing also acts as a backup thrust bearing due to the inclusion of thrust collars on the rotor. The bearings are a cageless, hybrid style with 52100 races and SiN3 balls and dry film lube (MoS2).

Steel sleeves are used for the rotor contacting surfaces. The backup bearings are carried by a radially compliant support in parallel with a friction damper.

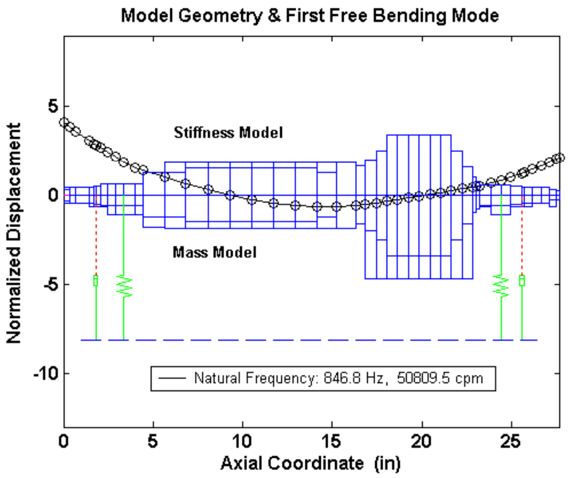

Fig. 3. Rotor Model Geometry & 1st Bending Mode.

3. System Dynamic Modeling

3.1 Rotordynamic Model

The rotordynamic structural model is shown in Figure 3. The top half shows the stiffness model and the lower half the mass model. The actuator and sensor locations and the first free/free, zero-speed bending mode are superimposed on the plot. The first four bending modes are included in the system analysis. The frequencies of those modes at zero speed are: 845 hz, 1530 hz, 1735 hz, and 2805 hz.

The rotordynamic equation of motion for the plant, which is in general a coupled, flexible rotor/casing system with conventional bearings, is:

$$[M]\{\ddot{q}\}+[C]\{\dot{q}\}+[K]\{q\}=\{f\} \qquad (1)$$

Where q represents the physical coordinate degrees of freedom, f represents external forces, and the mass matrix is represented by M. The passive negative stiffness of the magnetic bearing is included in the bearing stiffness matrix, K. The terms representing gyroscopic effects are part of the rotor partition of the damping matrix, C. For the flywheel, each rotor bending mode was given a static internal damping ratio of 0.25%. This is a conservative value for a rotor with sleeves if no modal test data is available.

For system analysis with magnetic bearings, the plant represented by Eqn. (1) is transformed to modal coordinates, m, and converted to state space form:

$$\begin{aligned}\{\dot{\mu}_P\}&=[A_P]\{\mu_P\}+[B_P]\{f\}\\ \{q\}&=[C_P]\{\mu_P\}+[D_P]\{f\}\end{aligned} \qquad (2)$$

Partitions of the characteristic matrix A_P contain the modal stiffness and damping matrices. The input and output matrices B_P and C_P contain mass normalized eigenvectors for modes selected for the system analysis. Some authors include the passive negative stiffness as part of the feed forward matrix D_P instead of as a bearing stiffness in K.

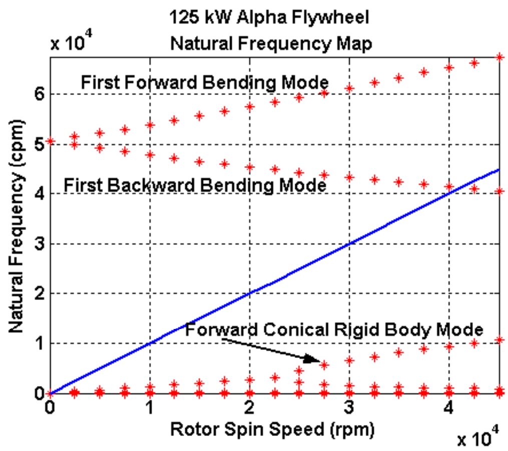

Fig. 4. Free/free Plant Natural Freq Map

A free/free plant natural frequency map is shown in Figure 4. The forward conical rigid body mode, ωn increases approximately with $\omega n = Ip/It * \omega s = 0.25 * \omega s$. This relatively small change with speed is a convenient characteristic that somewhat simplifies the magnetic bearing control scheme. The first bending mode, however, is quite gyroscopic because the flywheel hub, which has most of the polar inertia of the rotating assembly, must continually change its angular momentum vector to execute the mode (see Fig. 3).

3.2 Basic Magnetic Bearing Compensator

The basic magnetic bearing transfer function for Brg 1 is given in Figure 5. The transfer function for Brg 2 is similar. This is a single-input, single-output (SISO) transfer function. Although many gyroscopic systems require a MIMO system, the low rigid body Ip/It ratio of this flywheel allows the use of the simpler and less computationally intensive SISO transfer function. This is important for keeping DSP costs low. The control strategy provides direct phase lead for the second rigid body mode, and rolls off the compensation quickly enough to again provide phase lead for the backward and forward components of the first bending mode.

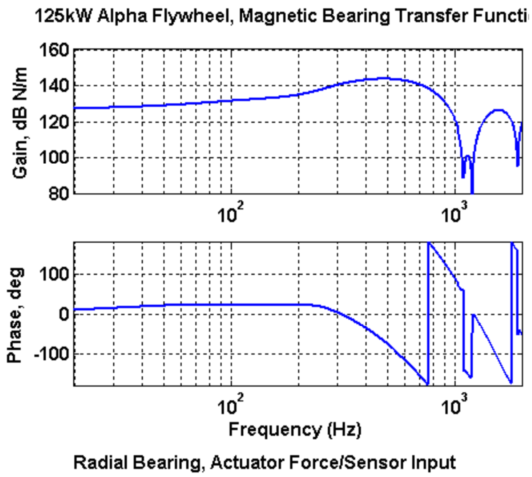

Fig. 5. Magnetic Bearing Transfer Function

3.3 System Analysis

For analysis, it is most convenient to convert the magnetic bearing transfer functions to state space form. They can then easily be coupled to the plant model for linear response and eigenvalue analysis. Table 2 is a summary of the closed loop eigenvalues for the two key modes of the flywheel, the forward conical mode and the backward bending mode. Gyroscopic effects are responsible for the rise of the second rotor rigid body mode with speed, as well as the spread of the forward and backward bending modes (see Figure 4).

3.4 Gain Scheduling Implementation

The gyroscopic effects on the rotor modes are best addressed using gain scheduling. This feature allows the use of a transfer function that is optimized more closely to the plant requirements within a given speed range than can be accomplished with a single control structure. Gain scheduling was implemented by structuring the control program to access up to four independent sets of control parameters (filter coefficients and gains). Each set of control parameters is applied in a different rotor spin speed range. The speed ranges overlap so that the selected set of control parameters is prevented from toggling back and forth near a transition speed. The three speed ranges actually used for the flywheel are indicated in Table 2. When the spin speed moves into a new speed range, the coefficients for that speed range are made current. The only hard limit to the number of speed ranges imposed by the control module is the amount of data memory used, which is about 1 kB per speed range with the structure now in use. The control parameters for the two higher speed ranges successively track the second forward rigid body mode and first backward bending mode, at the expense of reduced damping at lower frequencies (50-150 hz) since the critical speeds have already been traversed.

Table 2. Closed Loop Eig. for Key Modes.

	Forward Conical Mode		*1st Backward Bending Mode*	
Speed rpm	*Freq Hz*	*damping ratio*	*Freq Hz*	*damping ratio*
	Speed range 1, 0 – 19 krpm			
0	93.1	35.8%	829.0	1.46%
4000	106.1	27.5%	805.1	1.25%
8000	118.9	21.7%	782.9	0.87%
12000	137.5	13.9%	771.8	0.77%
16000	151.1	10.6%	752.6	0.45%
20000	165.1	8.4%	734.9	0.05%
	Speed range 2, 18 krpm – 28 krpm			
16000	130.7	7.9%	761.0	0.95%
20000	143.9	7.6%	743.1	0.84%
24000	157.8	8.3%	726.3	0.66%
28000	172.7	9.8%	710.5	0.43%
	Speed range 3, 27 krpm – 40 krpm			
24000	156.7	8.4%	731.9	0.75%
28000	171.2	9.9%	715.9	0.65%
32000	187.3	12.5%	700.8	0.49%
36000	207.8	18.7%	686.7	0.28%

3.5 Adaptive Open Loop Cancellation

Open loop cancellation (or adaptive vibration control) approaches have been widely described in the literature. There are numerous possible approaches, each with particular advantages. The choice depends on the system requirements and what is to be accomplished. The approach most often described adaptively minimizes synchronous displacement using a learned gain matrix that represents the force/displacement influence coefficients of the system. A second approach adaptively minimizes synchronous current, also using a learned gain matrix. A third approach adaptively minimizes the synchronous component of the error input to the DSP, thereby reducing synchronous current [6].

The second and third approaches most directly minimize synchronous current, and therefore reaction force, housing vibration, and power consumption. These two approaches make the most sense for flywheel energy storage systems. The second approach can be used through the rigid body mode traverse, so it has been used here up to 10,000 rpm. The third approach is the simplest, so it is applied here from 10,000 rpm to 36,000 rpm. This approach has much similarity to a tracking notch filter, and the similar limitation that it cannot be applied during the traverse of a mode This is because a synchronous force must be available from the bearings to counteract unbalance forces during the traverse of a mode.

4. Synchronous Response Data

Figures 6 - 9 show dynamic data collected from two runs of the Alpha flywheel. These runs were done with an unbalance weight of 635 gm-mm (25 gm-in) added at the combo bearing shaft end (Brg 2) to judge the effect of the synchronous cancellation algorithm. This single unbalance weight supplies a substantial modal unbalance for both of the forward rotor rigid body modes and the first rotor bending mode. The first set of data, collected without synchronous cancellation, is shown in Figures 6 & 7. This run was stopped at 27,000 rpm because the required dynamic current for the radial bearing (Brg 1) exceeded the slew rate limit of the bearing with the available overhead voltage. The dynamic load limit of the radial bearing is about 380 N at 450 hz (27,000 rpm). The displacement is well controlled as the bearing is quite stiff at that frequency - about 8750 N/mm (50,000 lb/in).

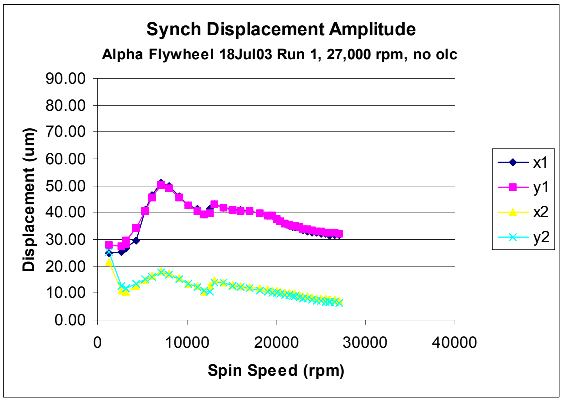

Fig 6. Synch Displacement, w/o cancellation

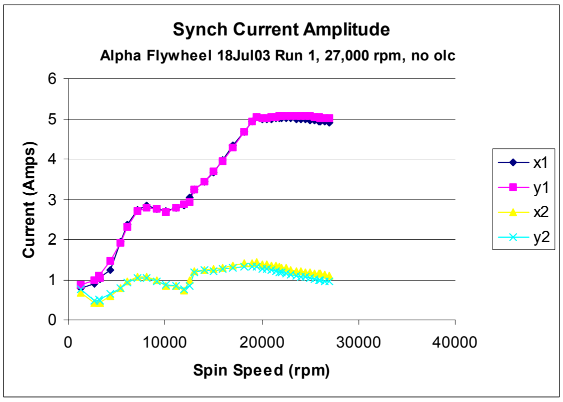

Fig 7. Synch Current, w/o cancellation

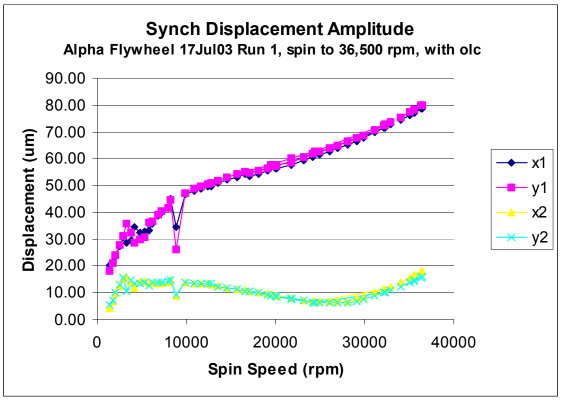

Fig 8. Synch Displacement, with cancellation

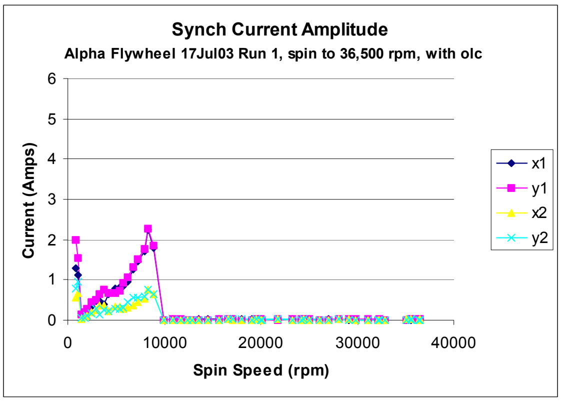

Fig 9. Synch Current, with cancellation

The second set of data, collected with synchronous cancellation active, is shown in Figures 8 & 9. Above 10,000 rpm, the synchronous cancellation algorithm is the synchronous input minimization type (no learned gain matrix). This approach lets the rotor spin about an inertial axis, which of course varies as the rotor speed changes. The synchronous current and therefore synchronous bearing load are effectively zero since the cancellation algorithm drives the input displacement to the controller to zero. This is beneficial for an energy storage flywheel, as it substantially reduces housing vibration and rotor eddy current losses. Rotor eddy current losses are reduced because no synchronous flux change is required for unbalance compensation.

5. Preliminary Thermal Analysis and Measurements

A key requirement for an energy storage flywheel is to minimize losses, which optimizes overall system storage efficiency. This drives the choice of vacuum operation to minimize windage losses, and magnetic bearings to minimize bearing losses. Minimizing losses that generate heat on the rotor then becomes particularly critical since any heat generated on the rotor must be radiated to the housing. This is because there is no mechanical contact and thus no convection or conduction path from rotor to housing. For this reason, the bearing and motor design must concentrate on minimizing rotor eddy current losses. Further, it is important to predict and measure the steady state rotor temperature, to ensure that a reasonable rotor temperature can be maintained. Desired target rotor temperature is 125°C, but the existing design is acceptable up to 150°C.

To this end, a series of long term tests under realistic operating conditions are planned to validate steady-state rotor temperature. Preliminary estimates of rotor losses and radiation heat transfer have also made to assess the reasonableness of the data and to guide future more detailed analysis and testing.

5.1 Rotor Temperature versus Time Data

The initial test performed is a 35 hour run at a constant 36,000 rpm. The motor was at idle, supplying just enough current to maintain the desired speed. The idle condition is a good initial test condition for this flywheel since it is designed to idle at 36,000 rpm for long periods with short bursts of power generation. Figure 10 shows a plot of the rotor temperature versus time during the test. The rotor temperature is approaching a steady state temperature of 98°C, a 67°C rise from the starting temperature of 31°C. This is well below the design target of 125°C very comfortable temperature for a steel rotor. Additional testing underway now will measure temperature rise using a number of charge/discharge cycles. The data can be well fitted by an exponential curve,

$$T = T_{final} - (T_{final} - T_{start})\, e^{(-t/\tau)} \quad (3)$$

where T is temperature, the subsripts start and final are the initial and steady-state temperatures respectively, t is time from the start, and τ is a time constant. As shown in Figure 10, a time constant of 9 hours provides a good fit to the data. The expression in Eqn. (3) is typical of systems that can be modeled as lumped systems with heat generation (a ball bearing temperature transient is another example).

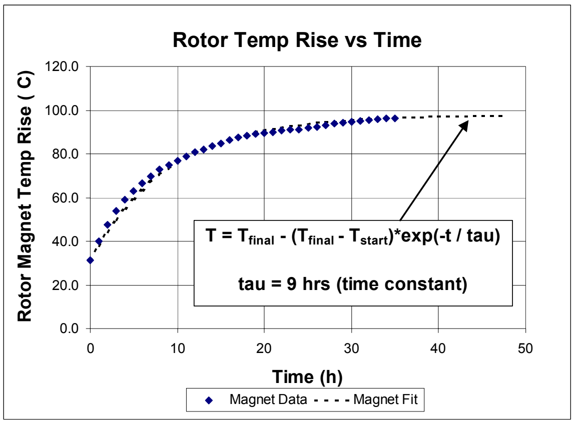

Fig. 10. Rotor Temperature Rise versus Time

5.2 Predicted Radiation Heat Transfer

When the steady-state temperature is reached, the power generated or lost on the rotor must equal the heat transfer from the rotor to the housing. A preliminary estimate of the steady state heat transfer was obtained from a simplified radiation heat transfer analysis. Given the steady state rotor temperature of 98°C, the steady state housing temperature of 44°C, estimates of the rotor and housing emissivities, and the geometry, potential heat transfer through radiation can be estimated. The predicted heat transfer is between 21 and 40 W, for rotor emissivities of 0.2 – 0.4. These emissivities are the typically published values for a dulled steel surface. The black oxide coated inner surface of the housing was taken as 0.8.

5.3 Predicted Rotor Losses

The actual losses on the rotor can also be predicted, again with large uncertainty, directly from the possible loss mechanisms. The main losses should come from motor eddy current losses and bearing eddy current losses. Windage was calculated and plotted, but is an insignificant contributor at the vacuum level used for the flywheel (10 mTorr). The results are shown in Figure 11, along with the estimated heat transfer from radiation.

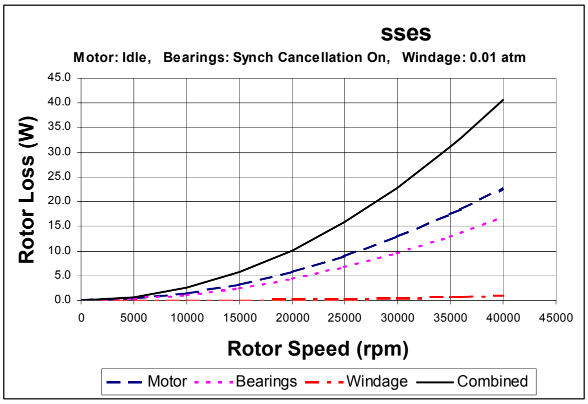

Fig 11. Predicted Rotor Losses

The source of the motor losses on the rotor is the slot ripple caused by the slots in the stator. The calculated losses depend on slot arc length, rotor/stator air gap, and slot ripple frequency. The magnetic bearing eddy current losses are similarly due to variation in the flux in the rotor laminations. The eddy current loss is proportional to the lamination thickness squared, the frequency squared, the flux density change squared, and is inversely proportional to the lamination resistivity. Hysteresis losses also occur in magnetic bearings and are related to the frequency and flux change to the 1.6 power. The hysteresis term is usually less important at the higher speeds found in a flywheel, but is included in the calculation presented here for the bearing losses. Windage losses can be calculated for all of the surfaces of the rotor and combined and is due to shearing of the air between the moving and stationary surface. It was assumed that half of the windage power loss goes into rotor heating, with the remainder heating the stator.

6. Conclusions

The development of an industrial energy storage flywheel module was described. A gain scheduled control strategy used for the magnetic bearings was discussed and response results presented. Synchronous response measurements showed the benefits of adaptive synchronous cancellation for reducing dynamic current and load. Preliminary rotor temperature versus time measurements show that the flywheel rotor steady state temperatures are under 100°C when idling at 36,000 rpm, well below the design target. Future testing will characterize temperature rise for various other loading cases.

References

[1] McMullen,P., Hawkins, L., Huynh, C., Dang, D., "Design and Development of a 100 kW Energy Storage Flywheel for UPS and Power Conditioning Applications", *Proc. of PCIM*, Nuremburg, Germany, May, 2003.

[2] Hayes, R.J., Kajs, J.P., Thompson, R.C., Beno, J.H., "Design and Testing of a Flywheel Battery for a Transit Bus", *SAE 1999-01-1159*, 1998.

[3] Hawkins, L.A., Murphy, B.T., Kajs, J.P., Analysis and Testing of a Magnetic Bearing Energy Storage Flywheel with Gain-Scheduled, MIMO Control, ASME 2000-GT-405, May, 2000.

[4] Hawkins,L., Murphy,B.,Zierer,J.,Hayes,R., "Shock and Vibration Testing of an AMB Supported Energy Storage Flywheel", *Proc. of 8th Intl. Symp. on Magnetic Bearings*, Mito, Japan, Aug, 2002.

[5] McMullen, P., Huynh, C., Hayes, R., "Combination Radial-Axial Magnetic Bearing", *Proc. of 7th Intl. Symposium on Magnetic Bearings*, Zurich, Switzerland, August, 2000.

[6] Larsonneur,R., Herzog,R., "Feedforward Compensation of Unbalance: New Results and Application Experiences", *Proc. IUTAM Symp. on Active Control of Vibration*, U. of Bath, UK, 1994.